HHS Public Access

Author manuscript

Nat Med. Author manuscript; available in PMC 2014 April 24.

Published in final edited form as:

Nat Med. ; 18(3): 396–404. doi:10.1038/nm.2629.

Activin–like kinase–3 activity is important for kidney regeneration and reversal of fibrosis

Hikaru Sugimoto[1], **Valerie S. LeBleu**[1], **Dattatreyamurty Basukonda**[2], **Peter Keck**[2], **Gangadhar Taduri**[1], **Wibke Bechtel**[1], **Hirokazu Okada**[1], **William Carlson Jr**[2,3], **Philippe Bey**[3], **Mary Rusckowski**[4], **Björn Tampe**[5], **Desiree Tampe**[5], **Keizo Kanasaki**[1], **Michael Zeisberg**[1,5], and **Raghu Kalluri**[1,5,6]

[1]Division of Matrix Biology, Department of Medicine, Beth Israel Deaconess Medical Center and Harvard Medical School, Boston, MA

[2]Thrasos Innovation Inc., Montreal, Quebec

[3]Division of Cardiology, Department of Medicine, Mass General Hospital/Harvard Medical School, Boston, MA

[4]Division of Nuclear Medicine, Department of Radiology, University of Massachusetts Medical College, Worcester, MA

[5]Department of Nephrology and Rheumatology, Goettingen University Medical Center, Georg August University, Goettingen, Germany

[6]Harvard–MIT Division of Health Sciences and Technology, Boston, MA

[7]Department of Biological Chemistry and Molecular Pharmacology, Harvard Medical School, Boston MA.

Abstract

Molecules associated with TGF-β superfamily such as BMPs and TGF-β are key regulators of inflammation, apoptosis and cellular transitions. Here, we demonstrate that the BMP receptor activin–like kinase 3 (Alk3) is elevated early in response to kidney injury and its deletion in the tubular epithelium leads to enhanced TGF-β1 / Smad3 signaling, epithelial damage and fibrosis, suggesting a protective role for Alk3 mediated signaling. Structure–function analysis of Alk3 / BMP / BMPRII ligand–receptor complex coupled with synthetic organic chemistry led us to

Address for Correspondence: Raghu Kalluri, MD, PhD Professor of Medicine Harvard Medical School Division of Matrix Biology Department of Medicine Beth Israel Deaconess Medical Center Boston, MA 02215 Tel: (617) 735–4601 rKalluri@BIDMC.Harvard.edu.

Author contributions:

RK–conceptually designed strategy for this study, participated in discussions, provided intellectual input, supervised the studies and wrote the manuscript. HS–performed experiments and analyzed the data. MZ–participated in the discussions and performed experiments. WB, PK, DB, WC, MR, PB, GT, AH, HO, DT, BT, VSL–performed experiments, analyzed the data and edited the manuscript and generated the figures. KK and VSL–supervised *in vitro* experiments, helped in the writing of the manuscript and generated the figures.

COMPETING FINANCIAL INTERESTS:

PK, DB, RK, WCjr and PB– Hold equity in Thrasos, Inc

HS, MZ, GT, AH, HO, DT, BT, VSL, MR and KK – No conflicts.

construct a library of small peptide agonists of BMP signaling that function via Alk3 receptor. One such peptide agonist, THR–123, suppressed inflammation, apoptosis epithelial–to–mesenchymal transition program, and reversed fibrosis in mouse models of acute and chronic injury. Combining THR–123 and angiotensin–converting enzyme inhibitor, captopril, exhibited additive therapeutic benefit in controlling fibrosis. Our studies demonstrate that BMP signaling agonists constitute a new line of therapeutic agents with a potential utility in the clinic to induce regeneration, repair and reverse fibrosis.

Introduction

Bone morphogenetic protein–7 (BMP7), a member of the transforming–growth factor (TGF)-β superfamily, acts as an antagonist of TGF-β–mediated activity[1-3]. BMP7 binds to three type I receptors, activin–like kinase (Alk) –2, –3, –6 and a type II receptor, BMPR–II, and displays distinct activities in different cell types[4], exhibiting anti–inflammatory and anti–apoptotic functions as well as promoting bone formation[5,6]. It is essential that BMPs interact with both type I and type II receptors for signaling and ligand–induced activation induces intrinsic serine / threonine kinase activity that triggers phosphorylation of receptor–regulated Smads (R–Smads). Smad2 and Smad3 are phosphorylated by type I receptors of TGF-β and activin, while Smad1, Smad5 and Smad8, act downstream of BMP type I receptors[4]. High affinity receptors for BMP7 are shown to be present in kidney epithelial cells, and are speculated to mediate BMP7 actions in the kidney[7,8].

End stage renal disease (ESRD) of various etiologies exhibit a positive correlation with the degree of tubulo–interstitial fibrosis[9-13]. Here we demonstrate that Alk3 functions to inhibit fibrosis by controlling inflammation, apoptosis and induction of an epithelium–to–mesenchymal (EMT) program. Peptide agonists of BMP signaling that bind to Alk3 were generated and one such peptide, THR–123, controls fibrosis and induces kidney regeneration.

Results

Alk3 is a negative regulator of fibrosis

Reno–protective properties and anti–fibrotic effects of BMP7 have been demonstrated in various kidney disease models[2,14-16], and BMP7 expression is suppressed in acute and chronic kidney injury[17-20]. We evaluated the expression levels of several BMP7 targets in mice with chronic renal injury over time. Alk3 expression uniquely peaked after only one week following kidney injury, and remained high between three to six weeks following injury when compared to control kidneys (**Fig. 1a, Supplementary Fig. 1a, b**). At week 9, Alk3 expression decreased when compared to control kidney (**Fig. 1a**), likely as a result of depletion of Alk3 expressing cells. In contrast, BMP7 expression levels decreased the most among all the molecules tested following kidney injury, reaching its minimum level at three weeks following injury and remained low (**Fig. 1a, Supplementary Fig. 1a, b**).

In mice with nephrotoxic serum induced chronic kidney fibrosis (NTN) (**Fig. 1b**), phosphorylated Smad1 (p–Smad1) accumulated in the nucleus of the tubules at week 1

following injury. Interestingly, p–Smad1 labeling decreased at week 6 post kidney injury (**Fig. 1c**), presenting a similar trend as that observed with Alk3 expression (**Fig. 1a**). These results further suggest that BMP7 / Alk3 axis correlates negatively with renal epithelial injury and interstitial fibrosis. To functionally address this observation, we deleted Alk3 receptor in the tubular epithelial cells.

We confirmed the specificity of γGT–Cre expression utilizing the R26R–Rosa–LSL–LacZ mice[21]. Reporter analysis revealed that γGT–Cre; R26R–Rosa–LSL–LacZ mice exhibit strong expression of LacZ in the proximal kidney tubules when compared to littermate control mice [Cre (–); R26R–Rosa–LSL–LacZ mice] (**Fig. 1d**). LacZ was not expressed in other organs, including the liver and hematopoietic compartment of these reporter mice (γGT–Cre; R26R–Rosa–LSL–LacZ mice) (**Supplementary Fig. 1** and data not shown).

Crossing of γGT–Cre mice with floxed alleles of Alk3 resulted in the excision of exon3 in the Alk3 gene, leading to the absence of Alk3 protein expression in kidney tubule compared to control Akk3 f/f mice without Cre–recombinase activity[22,23] (**Fig. 1e**). NTN induced severe crescentic glomerulonephritis with interstitial fibrosis initially in all groups of mice analyzed (**Fig. 1f**). Six weeks after the induction of NTN, fibrosis was more severe in γGT–Cre; Akk3 f/f mice (Alk3 deleted mice) compared to control mice (**Fig. 1f**). F4/80^{+} macrophage express Alk3, and such expression remained intact despite deletion of Alk3 using γGT–Cre mice, confirming that the accelerated fibrosis observed in these mice is reflective of the deletion of Alk3 in proximal tubules (**Supplementary Fig. 1d**). Such accelerated fibrosis in the Alk3 deleted mice was associated with enhanced activation of TGF-β pathway, as demonstrated by the increased p–Smad2 in the nucleus of the tubular epithelial cells (**Supplementary Fig. 1e**). Renal function as judged by blood urea nitrogen (BUN) measurement was significantly higher in the Alk3 deleted mice with fibrosis when compared to the control mice (**Fig. 1g**). This phenotype was not observed in γGT–Cre mice and unchallenged γGT–Cre; Akk3 f/f mice (**Supplementary Fig. 1f–g**).

Inflammation associated with macrophage influx and renal epithelial apoptosis are considered to be important instigators of renal fibrosis[24] . Mice with Alk3 deletion in the kidney tubular epithelium demonstrated increased influx of macrophages in association with fibrosis (**Supplementary Fig. 1h**). Increased number of tubular epithelial cells exhibited co–localization of both epithelial marker E–cadherin and mesenchymal marker, FSP1 (S100A4), indicative of an EMT program (**Fig. 1h**).

Design of the BMP signaling pathway agonists

Cyclic peptide agonists of the BMP signaling pathway were designed by identifying regions of the 3-D structure of TGF-β2[25,26] and BMP7[27] most likely involved in receptor interactions and by comparing side chain solvent accessibility with the regions of the TGF-β super family aligned sequences having the highest variability[27]. To further refine the regions of interest, we used a structure–variance analysis (SVA) program [28] that weighs physical–chemical residue properties at each position based on their correlation with an activity. The goal was to identify receptor–binding regions and then optimize the sequence for specific BMP activities. The highest scoring residue positions were then mapped onto the 3-D

structure of BMP7[27]. Of the three structural regions identified [27], peptides designed around the finger 2 loop proved to be the most promising. These are 16 residue long peptides of ~2 kDa molecular weight that are cyclized via a disulfide bond between the first and 11th residue positions in order to stabilize loop and preserve a 3-D conformation similar to the conformation in the finger 2 loop of BMP7 (**Fig. 2a**).

Preliminary screening for optimization was based on anti–inflammatory efficacy in an *in vitro* cell–based assay using a human renal tubular epithelial cell line (HK–2). The assay tested the ability of compounds to reverse the increase in the production of cytokine IL–6 that resulted from stimulation of the cells with tumor necrosis factor (TNF)-α (**Supplementary Fig. 1i**). Sequence–activity analysis was carried out using the SVA program. After six optimization cycles, a couple of compounds emerged as the lead candidates. One such candidate, THR–123 (**Fig. 2a**), was further evaluated in other relevant receptor-binding and anti–fibrosis assays.

First, we analyzed specific binding of the extra cellular domains (ECD) of the several type I receptors of BMPs to THR–123. Binding of cold BMP7 to immobilized receptor ECDs was determined by competition with ^{125}I–labeled BMP7 and analyzed by scatchard analysis to determine effective dissociation constants of BMP7 for each of the receptor ECDs. To obtain an estimate of the effective dissociation constant of THR–123 for a particular receptor ECD, the dissociation constant for cold BMP7 was multiplied by the ratio of the ED_{50} of THR–123 to the ED_{50} for cold BMP7. The data demonstrated that THR–123 competes with BMP7 for Alk3 and to some extent with Alk2 (data not shown), whereas absolutely no competition was observed with Alk6 (**Fig. 2b**), suggesting that of the three known BMP type I receptors, Alk3 is the predominant target for THR–123. The ~10^4 ratio of competitive EC_{50} binding of THR–123 to that of BMP7 with Alk3 is likely due to three effects: first, BMP7 binds as a dimer to two type I receptor ECD's (they are cloned as two copies for each Fc fragment), whereas, monomeric THR–123 binds to one type I receptor, therefore its affinity is the square root of the observed dimer affinity. Second, due to the difference in size of the molecules (the molecular weight of BMP7 dimer is ~19 times greater than THR–123), the available surface area of the BMP7 monomer is ~3 times that of the THR–123 monomer; and finally, when a weakly binding compound competes with a stronger one, the ratio of the EC_{50}'s overestimates the ratio of the K_D's by a factor of 2. Although these results do not inform on the *in situ* binding affinity of the peptides to native BMP receptors, they however support selective binding capacity of THR–123 to Alk3 and Alk2 but not Alk6.

The stability of THR–123 in whole blood and plasma was tested *in vitro*. In PBS–mannitol buffer, THR–123 was stable for over 400 minutes (**Fig. 2c**). In rat plasma, THR–123 is slowly degraded with a half–life of 358 minutes, while in whole blood, THR–123 degraded rapidly (half–life of 70 minutes) (**Fig. 2c**). The persistence of THR–123 in systemic circulation was evaluated using i.v. administered ^{125}I–labeled compound and following the radioactivity decay. In both plasma and whole blood, THR–123 levels immediately decreased within 5 minutes (by almost 90%), suggesting a very short half–life of THR–123 in the alpha–phase (**Fig. 2d**). Beta–phase assessment of ^{125}I–THR–123 indicates a half–life of 55–58 min (**Fig. 2e**). Six hours after intravenous administration of ^{125}I–THR–123, the

majority of the radioactivity was still localized in the kidney and bladder (**Fig. 2f**), suggesting that THR–123 accumulates in the kidney and is excreted, via the bladder, into the urine. Orally administrated ^{125}I–labeled THR–123 localized primarily to the kidney cortex within one hour after ingestion and peaked at about 3 hours (**Fig. 2g**). Twenty–four hours after ingestion, most of the ^{125}I–THR–123 associated radioactivity was cleared from the kidney (**Fig. 2g**).

THR–123 inhibits inflammation, apoptosis and EMT Program

Inflammation is a key feature in renal fibrosis. BMP7 displays an anti–inflammatory activity[6,29], thus prompting us to investigate the effect of THR–123 on the expression of several pro–inflammatory cytokines in human renal tubular epithelial cell line (HK–2 cells). BMP7 and THR–123 inhibited TNF-α induced IL–6 production in dose dependent manner (**Supplementary Fig. 2a**). THR–123 also inhibits TNF-α–induced IL–8 and ICAM–1 production in HK–2 cells (**Supplementary Fig. 1a**), suggesting that similar to the function of BMP7, THR–123 exhibits anti–inflammatory properties.

BMP7 is also reported to protect tubular epithelial cells (TECs) from apoptosis[18]. TGF-β–induced apoptosis in TECs was analyzed by Annexin V labeling (**Supplementary Fig. 2b**). BMP7 and THR–123 exhibited similar anti–apoptotic activity, while such anti–apoptotic activity was not detected when a control scrambled cyclic peptide was used (**Supplementary Fig. 2b, c**). Hypoxia induced apoptosis of TECs was also inhibited by BMP7 and THR–123 **(Supplementary Fig. 2c**). Additionally, cisplatin induced apoptosis was inhibited by THR–123 (**Supplementary Fig. 2d**).

BMP7 has been shown to inhibit TGF-β induced epithelial–to–mesenchymal transition (EMT) program[2]. Similar to BMP7, THR–123 inhibited TGF-β induced EMT program (**Supplementary Fig. 3**). TGF-β inhibited E–cadherin expression, while both BMP7 and THR–123 restored TGF-β–suppressed E–cadherin to normal levels (**Supplementary Fig. 3b, c**). Control cyclic scrambled peptide exhibited insignificant effect on the EMT program (**Supplementary Fig. 3a, b)**. Such effect of THR–123 is associated with Smad1/5 phosphorylation (p-Smad1/5) **(Supplementary Fig. 3d).** TGF-β induced expression of genes associated with EMT program such as snail (*Sna*) and *CTGF* was inhibited by THR–123 (**Supplementary Fig. 3e**). After 48 hours of incubation with TGF-β and epidermal growth factor (EGF), TECs exhibited mesenchymal features indicative of EMT (**Supplementary Fig. 3f, g**). The TGF-β–induced EMT in these cells was reversed by the treatment with BMP7 or THR–123 (**Supplementary Fig. 3f–h**). Control peptide revealed insignificant effect on EMT induction (**Supplementary Fig. 3f–h**). THR–123–induced reversal of EMT was associated with restoration of E–cadherin expression (**Supplementary Fig. 3g)**.

THR–123 induces regeneration and reverses fibrosis

We analyzed the effect of THR–123 on acute renal injury using the ischemic re–perfusion injury (IRI) model in mice. Seven days after IRI, control mice exhibited renal morphology consistent with acute renal tubular necrosis characterized by tubular dilatation and flattened epithelial cells with eosinophilic homogenous cytoplasm (**Supplementary Fig. 4a**). THR–

123–treated mice displayed significantly less tubular damage in IRI kidney when compared to control mice, yet blood urea nitrogen levels were similar in both groups (**Supplementary Fig. 4a**).

Unilateral ureteral obstruction (UUO) is a well–established model of severe renal interstitial injury and fibrosis (**Supplementary Fig. 4b**). Five days after UUO, kidneys display significantly increased interstitial volume when compared to normal kidney (**Supplementary Fig. 4b**). Oral administration of THR–123 (5 mg.Kg^{-1} or 15 mg.Kg^{-1}) inhibited interstitial volume expansion in UUO kidneys when compared to untreated mice (**Supplementary Fig. 4b**). Seven days after UUO, kidneys exhibited severe fibrosis with increased interstitial volume (**Supplementary Fig. 4b**). Intraperitoneal administration of BMP7 ameliorated interstitial volume expansion when compared to control mice (**Supplementary Fig. 4c**). Both intraperitoneal and oral administration of THR–123 inhibited fibrosis (**Supplementary Fig. 4c**). Decreased tubular damage with THR–123 treatment was associated with decreased expression of matrix components such as fibronectin (*Fn1*) and type I collagen (*Col4a1*) (**Supplementary Fig. 4d**).

We next analyzed the effect of THR–123 on the nephrotoxic nephritis induced by sheep anti–glomerular antibodies (NTN) model. Kidneys with NTN exhibit severe crescentic glomerulonephritis with interstitial damage and fibrosis[1,30]. Such lesions develop in a progressive manner in the CD–1 mice (**Fig. 3a, Supplementary Fig. 5a**). Six weeks following NTN induction, mice exhibited severe crescentic glomerulonephritis with severe interstitial damage and fibrosis (**Fig. 3b**). THR–123 treatment (initiated at six weeks following NTN induction) improved glomerular lesion (sclerosis) and tubular atrophy and fibrosis (**Fig. 3b**), associated with decreased expression of matrix components such as fibronectin (*Fn1*) and type I collagen (*Col4a1*) (**Supplementary Fig. 5b**). Blood urea nitrogen was decreased after THR–123 treatment (**Fig. 3c**). We identified tubular cells with EMT program, as being positive for both FSP1 and E–cadherin. Similar to previous reports[2], EMT program was evident in NTN kidneys when compared to normal kidney (**Fig. 3d**). THR–123 treatment significantly decreased the number of cells exhibiting an EMT program (**Fig. 3d**). NTN kidneys exhibited increased Mac–1 and F4/80 positive macrophages when compared to control normal kidney; and THR–123 treatment inhibited accumulation of macrophage (**Supplementary Fig. 5c, d**). THR–123 treated kidneys presented with increased accumulation of p-Smad1/5, revealing a possible stimulation of Alk3–mediating pathway (**Supplementary Fig. 5e**).

Alport syndrome is a inherited kidney disease caused by genetic mutations in genes encoding for type IV collagen proteins[31]. The mice deficient in alpha 3 chain of type IV collagen chain (COL4A3KO mice) mimic renal disease associated with Alport syndrome. At 16 weeks of age, COL4A3KO mice exhibited increased glomerular abnormality, tubular atrophy and fibrosis when compared to wild–type kidney (**Supplementary Fig. 6a**). While THR–123 treatment did not alter glomerular abnormalities (**Supplementary Fig. 6a–b**), it significantly inhibited tubular atrophy and interstitial fibrosis (**Supplementary Fig. 6a–b**). Blood urea nitrogen levels were increased in COL4A3KO mice when compared to wild–type mice and THR–123 significantly improved blood urea nitrogen level in COL4A3KO

mice (**Supplementary Fig. 6b**). In COL4A3KO kidney, the number of cells exhibiting EMT program was significantly higher when compared to wild–type kidney (**Supplementary Fig. 6d).** THR–123 treatment inhibited such acquisition of an EMT program (**Supplementary Fig. 6e**). Macrophage infiltration in COL4A3KO kidney was increased when compared to control kidney and THR–123 treatment inhibited macrophage infiltration (**Supplementary Fig. 6e**). THR–123 treated COL4A3KO kidneys were associated with an increase in p–Smad1/5 (**Supplementary Fig. 6f**).

Next, we evaluated the efficacy of THR–123 in controlling diabetic nephropathy (DN) in mice. CD–1 mice injected with streptozotocin (STZ) exhibit increased glomerular mesangial matrix with increased glomerular surface area associated with interstitial damages by six months when compared to control mice, suggesting advanced DN (**Fig. 4a, Supplementary Fig. 7a**). While neither BMP7 nor THR–123 inhibited glomerular surface area increase in diabetic mice, both BMP7 and THR–123 inhibited mesangium expansion in STZ–induced six month DN (**Fig. 4b**). Furthermore, THR–123 treatment (5–6 months) substantially reversed mesangial matrix expansion when compared to mice with five months of DN (before THR–123 administration began) (**Fig. 4b**). DN mice displayed increased tubular atrophy and interstitial volume when compared to control mice (**Fig. 4b**). Treatment with BMP7 (1–6 months treatment) or THR–123 (5–6 months treatment) inhibited tubular atrophy and interstitial volume increase (**Fig. 4b**). THR–123 substantially reversed tubular atrophy and interstitial volume expansion (**Fig. 4b**). Blood urea nitrogen levels increased in DN when measured at five and six month following STZ administration (**Fig. 4c**). Both BMP7 and THR–123 significantly reversed renal dysfunction in DN (**Fig. 4c**), inhibited induction of an EMT program (**Fig. 4d**), and reduced macrophage infiltration (**Supplementary Fig. 7b, c**). THR–123 treated kidneys of mice with DN were also associated with increased accumulation of p-Smad1/5 (**Supplementary Fig. 7d**).

Angiotensin–converting enzyme inhibitor (ACE–I) is a well–established drug used to control progression of several chronic progressive kidney diseases including diabetic nephropathy[32,33]. Therefore, we tested THR–123 and ACE–I [captopril (CPR)] in combination in mice with advanced diabetic kidney disease associated fibrosis. Seven months after induction of diabetes, DN kidneys displayed a significant increase in glomerular surface area and mesangial matrix deposition (**Fig. 5a**). CPR and CPR / THR–123 combination treatment was initiated in mice with severe DN at seven months following DN induction. Glomerular surface area remained identical in all groups analyzed (**Fig. 5b**). CPR treatment did not inhibit progression of mesangial matrix expansion in these experiments, but a combination of CPR with THR–123 significantly reduced mesangial expansion and substantially reversed it when compared to untreated control mice (**Fig. 5b**). Between seven to eight months (late–stage) after induction of diabetes, DN kidney exhibited tubular atrophy and interstitial volume expansion (**Fig. 5b**). CPR alone partially inhibited tubulo–interstitial alterations in DN kidney while a combination of CPR with THR–123 completely inhibited tubular atrophy and interstitial volume expansion (**Fig. 5b**). Blood urea nitrogen level analysis revealed that DN mice exhibit significant renal function deterioration between seven and eight months after induction of diabetes (**Fig. 5c**). CPR did not (P = 0.08), but combination therapy significantly inhibited the progressive loss of renal function

(**Fig. 5c**). EMT program was inhibited by CPR alone and also by the CPR / THR–123 combination treatment (**Fig. 5d**). Both CPR and CPR / THR–123 combination therapy inhibited macrophage infiltration (**Supplementary Fig. 7e**). CPR significantly inhibited apoptosis in diabetic kidney and CPR / THR–123 combination therapy exhibited additive anti–apoptotic effects (**Supplementary Fig. 7f**). CPR / THR–123 treated kidneys were associated with increased accumulation of p–Smad1/5 (**Supplementary Fig. 7g**). Blood sugar level and body weight were not altered in all the groups analyzed when compared to untreated diabetic mice at similar age (**Supplementary Fig. 7h, i**).

Loss of Alk3 prevents THR–123 activity

Binding of THR–123 to the Alk3 receptor induced actions that mimic BMP7 (*vide supra*). Our experiments suggested that THR–123 functions to suppress renal injury and fibrosis by inhibiting inflammation, apoptosis and EMT program. To functionally validate the target of THR–123 in exerting such reno–protective activity in mice, we tested the efficacy of THR–123 in the Alk3 deleted mice subjected to renal injury. The Alk3 deleted mice and their littermate (control) mice were subjected to IRI. The mice with Alk3 deficiency exhibit accelerated acute renal injury when compared to the control mice (**Supplementary Fig. 8a**). THR–123 inhibited renal injury in the control mice but does not exhibit therapeutic effect in the Alk3 deleted mice (**Supplementary Fig. 8a**). Alk3 dependent action of THR–123 in the control mice was associated with the reduction in macrophage accumulation (**Supplementary Fig. 8b**) and decreased tubular apoptosis (**Supplementary Fig. 8c)**.

Accelerated renal failure and fibrosis was observed in Alk3 deleted mice with NTN when compared to the control mice (**Fig. 6a**). We demonstrate that while THR–123 was successful in controlling renal injury and fibrosis in the control mice, it has no efficacy in the Alk3 deleted mice (**Fig. 6a)**. Such therapeutic effects of THR–123 on control mice with NTN was associated with the inhibition of macrophage accumulation in the kidney and EMT program in the tubules, whereas THR–123 inhibited neither macrophage accumulation (**Fig. 6b**) nor induction of an EMT program (**Fig. 6c**) in Alk3 deleted mice with NTN. THR–123 inhibit apoptosis in wild type kidney with NTN but had no effect on apoptosis in Alk3 deleted mice (**Supplementary figure 8d**). Finally, THR–123 restored renal function in control mice with NTN, but such reno–protective effect of THR–123 was not realized in Alk3–deleted mice (**Fig. 6d**).

Discussion

TGF-β super–family proteins wield considerable influence on the pathogenesis of renal fibrosis[34]. Many of the molecules in this family, most importantly TGF-β1 and TGF-β2, have been identified as positive regulators of fibrosis due to their ability to recruit myofibroblasts, facilitate EMT program, influence inflammation and induce epithelial cell apoptosis[2,5,18,29]. While much focus has been placed on the positive role of TGF-β1 in fibrosis, BMP7 (another molecule in the TGF super–family) was found to inhibit and reverse fibrosis[2]. BMP7 action is realized via its anti–inflammatory, anti–apoptosis and EMT suppressive actions[2,5,18,29]. BMP7 counter–balances the actions of TGF-β1 via Smad–dependent pathways[2]. In this regard, BMP7 can also bind to Alk6 receptor on osteoblasts

and induce bone formation[35-38]. In the kidney, tubular epithelial cells predominantly express Alk3 receptor[39]. Therefore, an ideal therapeutic candidate would be one that binds to Alk3 but not to Alk6 receptor, induces BMP signaling but does not induce osteogenic activity. While the levels of BMP7 decreases in the context of renal injury, the role of Alk3 in the progression of renal disease is unknown[17–20]. Our results also suggested that expression of BMP7 and Alk3 inversely correlate with progression of fibrosis supporting the notion that BMP7 plays a likely reno–protective role, in opposition to TGF-β1 action[2]. Similarly, in this study we identify that Alk3 is also a positive regulator of renal health during injury. It responds to renal injury in a protective fashion and its loss augments the progression of renal fibrosis. These results, coupled with the anti–fibrotic activity of BMP7, provided the necessary rationale design a new class of molecules that serve as BMP signaling agonist via their binding to Alk3. One such candidate molecule, THR–123, was further tested for mechanism of action and therapeutic efficacy.

THR–123 suppressed progression of kidney disease and substantially reversed established kidney fibrosis without inducing any osteogenic activity. Interestingly, while Alk3 receptor expression likely decreases at end–stage kidney disease, THR–123 still exhibits substantial activity. This suggests that such diminished level of Alk3 in not a rate–limiting factor for the efficacy of THR–123. We show that a combination of THR–123 and captopril, an angiotensin converting enzyme inhibitor, had an additive therapeutic effect in controlling renal fibrosis associated with diabetic kidney disease. Collectively, our results indicate that THR–123 inhibits inflammation, apoptosis, EMT program and reverses renal fibrosis. It is possible that Alk2 receptor may also contribute to the action of THR–123, but experiments using genetic mouse model suggest that such Alk2 mediated activity, if present, is minimal.

In summary, our study suggests that Alk3 receptor is a negative regulator of fibrosis when kidney is injured. THR–123, a small peptide BMP signaling agonist that binds to Alk3 and activates the Smad pathway, demonstrates therapeutic efficacy when administered orally to mice with fibrosis. Such reno–protective properties mirrored the action of BMP7, the natural ligand of Alk3, in the kidney. These pre–clinical studies offer insights into the use of BMP signaling pathway agonists in the treatment of acute and chronic kidney injury.

Materials and Methods Summary

Mice

The Alk3 f/f mice were bred with γGT–Cre mice to generate mice with deletion of Alk3 receptors in proximal tubular cells. The γGT promoter used to generate the Cre expressing mice was designed to express predominantly in the kidney proximal and distal tubules, with undetectable expression in the liver. The mice were on Balb/C background. Type IV collagen α3 chain knockout mice (COL4A3KO, C57Bl/6 background) mice were previously described[31]. Nephrotoxic serum induced nephritis (NTN), ischemic reperfusion injury (IRI), unilateral ureteral obstruction (UUO), and diabetic nephropathy (DN) models are described in online method section. Dose and routes for treatment with THR–123, BMP7 and captopril (and combination therapy) are detailed in the online method section. All animal experiments were reviewed and approved by the Beth Israel Deaconess Medical Center Institutional Animal Care and Use Committee.

Synthesis and pharmacokinetics of THR–123

Radio–ligand receptor competitive binding assays of THR–123 for specific for individual type I receptors Alk3 and Alk6 was performed using highly purified extra–cellular domain (ECD) of Alk3 or Alk6 (expressed as a fusion protein with Fc domain) immobilized on each well. Peptide analog or unlabeled BMP7 was added, followed by ^{125}I–labeled BMP7. Radiolabeled BMP7 complex was counted in an auto–gamma counter. Unlabeled BMP7 served as a positive control in both assays. Concentration of THR–123 in systemic circulation of Wistar rats was performed by measuring total radioactivity using automatic gamma well counter in plasma and whole blood following i.v. injection of THR–123 (^{125}I–Tyr) via the tail vein. Freshly harvested rat blood (male Sprague–Dawley, 0.35kg body weight), plasma and PBS mannitol buffer solution were spiked with THR–123 at a final concentration of 0.1 mg.ml^{-1}. Blood, plasma and buffer tubes were incubated at 37 °C for up to 6 hours and duplicate samples of 500 μl (blood) and 250 μl (plasma and blood) were analyzed at 0, 7.5, 15, 30, 60, 120, 240 and 360 minutes following injection of THR–123. Samples were analyzed for THR–123 using an LC–MS–MS method having a limit of detection of 1 μg.ml^{-1}. For tissue distribution of THR–123, tissues were harvested six hours after i.v. administration of ^{125}I labeled THR–123 (^{125}I–THR–123) in rats at a dose of 6.25 mg.kg^{-1} body weight, and were analyzed by automatic gamma well counter. Elimination of THR–123 from the body following oral administration was evaluated by measuring radioactivity in the kidneys of rats orally administrated ^{125}I–THR–123 at a dose of 5 mg.kg^{-1} body weight.

Reagents

Monoclonal antibody for E–cadherin was purchased from BD Biosciences. Mac–1 antibody was purchased from AbD Serotec. F4/80 and BMP7 antibody was purchased from Abcam. p–Smad1/5 antibody was purchased from Cell Signaling Technology. Alk3 and E–cadherin antibodies were purchased from Santa Cruz Biotechnology. For western blot analyses, Alk3 antibody was purchased from EMD Millipore. Measurements of BUN were performed using the QuantiChrom™Urea Assay Kit (BioAssay System) or DIUR–500 QuantiChrom™ Urea Assay Kit (Gentaur). Measurements of urine albumin and urine creating were performed using the QuantiChrom™ Assay for albumin (DIAG-500) and creatinine (DICT-250) Kit (BioAssay System). Details for morphormetric analyses of histological findings are listed in the online method section.

Quantitative PCR analysis

Total RNA was isolated from the kidney by Trizol/Invitrogen PureLink RNA Mini Kit for RNA extraction. Ten nanograms of total RNA were used for generating complementary cDNA using the TaqMan One–Step RT–PCR Master Mix (Applied Biosystems). Quantitative PCR was performed to analyze the gene expression profile of listed genes using ABIprism 7,000 (Applied Biosystems). Gene list and primer sequences are listed in online method section.

Detection of LacZ

Kidney samples (1 mm^2) from six weeks–old R26R–Rosa–LSL–LacZ mice [23] with or without Cre–recominase expresssion were fixed at 4 °C for 4 hours in 4% paraformaldehyde. Samples were washed 3 times with PBS pH 7.3 and then stained overnight at 37 °C with LacZ staining buffer (1mg.ml^{-1} X–gal, 35 mM potassium ferrocyanide, 35 mM potassium ferricyanide, 2 mM $MgCl_2$, 0.02% NP–40, 0.01% sodium deoxycholate in PBS). After washing with PBS pH 7.3, samples were embedded into paraffin. Sections (10 μm) were then deparaffinized and counterstained with eosin.

Statistical analysis

The data were expressed as means ± s.e.m. Analysis of variance (ANOVA) followed by Bonferroni/Dunn's test for multiple comparisons of mouse samples were used to determine significance. Student's T–test analysis was used for single parameter comparisons. Statistical significance was defined as $P < 0.05$. Graph–pad Prism software was used for statistical analysis.

Supplementary Material

Refer to Web version on PubMed Central for supplementary material.

Acknowledgements

This study was supported by NIH Grants DK55001, DK061688, DK081576, DK074558, CA155370 CA163191, CA125550, CA151925 and the Else Kröner–Memorial–Stipend (MZ). VSL is funded from the Research Training Grant in Gastroenterology (2T32DK007760–11). HS is funded by the Research Training Grant in Cardiovascular Biology (5T32HL007374–30). Mice with Alk3 flox/flox allele (Alk3 f/f) were kindly provided by Dr. Yuji Mishina, US National Institute of Health under a material transfer agreement. γGT–Cre mice and NP–1 cells, and polyclonal antibody for FSP1 were provided by Dr. Eric Neilson, Vanderbilt University Medical Center. We thank Scott McGoohan for his technical assistance.

Reference

1. Zeisberg M, Kalluri R. The role of epithelial-to-mesenchymal transition in renal fibrosis. J Mol Med. 2004; 82:175–181. [PubMed: 14752606]
2. Zeisberg M, et al. BMP-7 counteracts TGF-beta1-induced epithelial-to mesenchymal transition and reverses chronic renal injury. Nat Med. 2003; 9:964–968. [PubMed: 12808448]
3. Zeisberg EM, et al. Endothelial-to-mesenchymal transition contributes to cardiac fibrosis. Nat Med. 2007; 13:952–961. [PubMed: 17660828]
4. Miyazono K, Maeda S, Imamura T. BMP receptor signaling: transcriptional targets, regulation of signals, and signaling cross-talk. Cytokine Growth Factor Rev. 2005; 16:251–263. [PubMed: 15871923]
5. Simic P, Vukicevic S. Bone morphogenetic proteins: from developmental signals to tissue regeneration. Conference on bone morphogenetic proteins. EMBO Rep. 2007; 8:327–331. [PubMed: 17363970]
6. Simic P, Vukicevic S. Bone morphogenetic proteins in development and homeostasis of kidney. Cytokine Growth Factor Rev. 2005; 16:299–308. [PubMed: 15923134]
7. Ishidou Y, et al. Enhanced expression of type I receptors for bone morphogenetic proteins during bone formation. J Bone Miner Res. 1995; 10:1651–1659. [PubMed: 8592941]
8. Bosukonda D, Shih MS, Sampath KT, Vukicevic S. Characterization of receptors for osteogenic protein-1/bone morphogenetic protein-7 (OP-1/BMP-7) in rat kidneys. Kidney Int. 2000; 58:1902–1911. [PubMed: 11044210]

9. Schainuck LI, Striker GE, Cutler RE, Benditt EP. Structural-functional correlations in renal disease. II. The correlations. Hum Pathol. 1970; 1:631–641. [PubMed: 5521736]
10. Striker GE, Schainuck LI, Cutler RE, Benditt EP. Structural-functional correlations in renal disease. I. A method for assaying and classifying histopathologic changes in renal disease. Hum Pathol. 1970; 1:615–630. [PubMed: 5521735]
11. Risdon RA, Sloper JC, de Wardener HE. Relationship between renal function and histological changes found in renal biopsy specimens from patients with persistent glomerular nephritis. Lancet. 1968; 2:363. [PubMed: 4173786]
12. Nath KA. Tubulointerstitial changes as a major determinant in the progression of renal damage. Am J Kidney Dis. 1992; 20:1–17. [PubMed: 1621674]
13. Mackensen-Haen S, Bader R, Grund KE, Bohle A. Correlations between renal cortical interstitial fibrosis, atrophy of the proximal tubules and impairment of the glomerular filtration rate. Clin Nephrol. 1981; 15:167–171. [PubMed: 7237863]
14. Sugimoto H, Grahovac G, Zeisberg M, Kalluri R. Renal fibrosis and glomerulosclerosis in a new mouse model of diabetic nephropathy and its regression by bone morphogenic protein-7 and advanced glycation end product inhibitors. Diabetes. 2007; 56:1825–1833. [PubMed: 17456853]
15. Zeisberg M, Shah AA, Kalluri R. Bone morphogenic protein-7 induces mesenchymal to epithelial transition in adult renal fibroblasts and facilitates regeneration of injured kidney. J Biol Chem. 2005; 280:8094–8100. [PubMed: 15591043]
16. Zeisberg M, et al. Bone morphogenic protein-7 inhibits progression of chronic renal fibrosis associated with two genetic mouse models. Am J Physiol Renal Physiol. 2003; 285:F1060–1067. [PubMed: 12915382]
17. Tuglular S, et al. Cyclosporine-A induced nephrotoxicity is associated with decreased renal bone morphogenetic protein-7 expression in rats. Transplant Proc. 2004; 36:131–133. [PubMed: 15013323]
18. Wang SN, Lapage J, Hirschberg R. Loss of tubular bone morphogenetic protein-7 in diabetic nephropathy. J Am Soc Nephrol. 2001; 12:2392–2399. [PubMed: 11675415]
19. Vukicevic S, et al. Osteogenic protein-1 (bone morphogenetic protein-7) reduces severity of injury after ischemic acute renal failure in rat. J Clin Invest. 1998; 102:202–214. [PubMed: 9649574]
20. Simon M, et al. Expression of bone morphogenetic protein-7 mRNA in normal and ischemic adult rat kidney. Am J Physiol. 1999; 276:F382–389. [PubMed: 10070161]
21. Srinivas S, et al. Cre reporter strains produced by targeted insertion of EYFP and ECFP into the ROSA26 locus. BMC Dev Biol. 2001; 1:4. [PubMed: 11299042]
22. Mishina Y, Hanks MC, Miura S, Tallquist MD, Behringer RR. Generation of Bmpr/Alk3 conditional knockout mice. Genesis. 2002; 32:69–72. [PubMed: 11857780]
23. Iwano M, et al. Evidence that fibroblasts derive from epithelium during tissue fibrosis. J Clin Invest. 2002; 110:341–350. [PubMed: 12163453]
24. Rodriguez-Iturbe B, Garcia Garcia G. The role of tubulointerstitial inflammation in the progression of chronic renal failure. Nephron Clin Pract. 2010; 116:c81–88. [PubMed: 20502043]
25. Schlunegger MP, Grutter MG. An unusual feature revealed by the crystal structure at 2.2 A resolution of human transforming growth factor-beta 2. Nature. 1992; 358:430–434. [PubMed: 1641027]
26. Daopin S, Piez KA, Ogawa Y, Davies DR. Crystal structure of transforming growth factor-beta 2: an unusual fold for the superfamily. Science. 1992; 257:369–373. [PubMed: 1631557]
27. Griffith DL, Keck PC, Sampath TK, Rueger DC, Carlson WD. Three- dimensional structure of recombinant human osteogenic protein 1: structural paradigm for the transforming growth factor beta superfamily. Proc Natl Acad Sci U S A. 1996; 93:878–883. [PubMed: 8570652]
28. Keck, PC. Computer Method And Apparatus For Classifying Objects. 2002. WO/2002/037313
29. Gould SE, Day M, Jones SS, Dorai H. BMP-7 regulates chemokine, cytokine, and hemodynamic gene expression in proximal tubule cells. Kidney Int. 2002; 61:51–60. [PubMed: 11786084]
30. Lloyd CM, et al. RANTES and monocyte chemoattractant protein-1 (MCP-1) play an important role in the inflammatory phase of crescentic nephritis, but only MCP-1 is involved in crescent formation and interstitial fibrosis. J Exp Med. 1997; 185:1371–1380. [PubMed: 9104823]

31. Kashtan CE. Alport syndrome. An inherited disorder of renal, ocular, and cochlear basement membranes. Medicine (Baltimore). 1999; 78:338–360. [PubMed: 10499074]
32. Parving HH, Hommel E, Damkjaer Nielsen M, Giese J. Effect of captopril on blood pressure and kidney function in normotensive insulin dependent diabetics with nephropathy. Bmj. 1989; 299:533–536. [PubMed: 2507061]
33. Lewis EJ, Hunsicker LG, Bain RP, Rohde RD. The effect of angiotensin-converting-enzyme inhibition on diabetic nephropathy. The Collaborative Study Group. N Engl J Med. 1993; 329:1456–1462. [PubMed: 8413456]
34. Border WA, Noble NA. Transforming growth factor beta in tissue fibrosis. N Engl J Med. 1994; 331:1286–1292. [PubMed: 7935686]
35. Hojo H, Ohba S, Yano F, Chung UI. Coordination of chondrogenesis and osteogenesis by hypertrophic chondrocytes in endochondral bone development. J Bone Miner Metab. 2010; 28:489–502. [PubMed: 20607327]
36. Archdeacon P, Detwiler RK. Bone morphogenetic protein 7 (BMP7): a critical role in kidney development and a putative modulator of kidney injury. Adv Chronic Kidney Dis. 2008; 15:314–320. [PubMed: 18565482]
37. Haaijman A, et al. Correlation between ALK-6 (BMPR-IB) distribution and responsiveness to osteogenic protein-1 (BMP-7) in embryonic mouse bone rudiments. Growth Factors. 2000; 17:177–192. [PubMed: 10705576]
38. Ide H, et al. Growth regulation of human prostate cancer cells by bone morphogenetic protein-2. Cancer Res. 1997; 57:5022–5027. [PubMed: 9371496]
39. Wetzel P, et al. Bone morphogenetic protein-7 expression and activity in the human adult normal kidney is predominantly localized to the distal nephron. Kidney Int. 2006; 70:717–723. [PubMed: 16807538]
40. Strutz F, et al. Identification and characterization of a fibroblast marker: FSP1. J Cell Biol. 1995; 130:393–405. [PubMed: 7615639]
41. Strutz F, et al. TGFb1 induces proliferation in human renal fibroblasts via induction of basic fibroblast growth factor (FGF–2). Kidney International. 2001; 59:579–592. [PubMed: 11168939]
42. Koziolek MJ, et al. Role of CX3C–chemokine CX3C–L/fractalkine expression in a model of slowly progressive renal failure. Nephrol Dial Transplant. 2010; 25:684–698. [PubMed: 19934081]
43. Haverty TP, et al. Characterization of a renal tubular epithelial cell line which secretes the autologous rarget antigen of autoimmune experimental interstitial nephritis. J Cell Biol. 1988; 107:1359–68. [PubMed: 3170633]

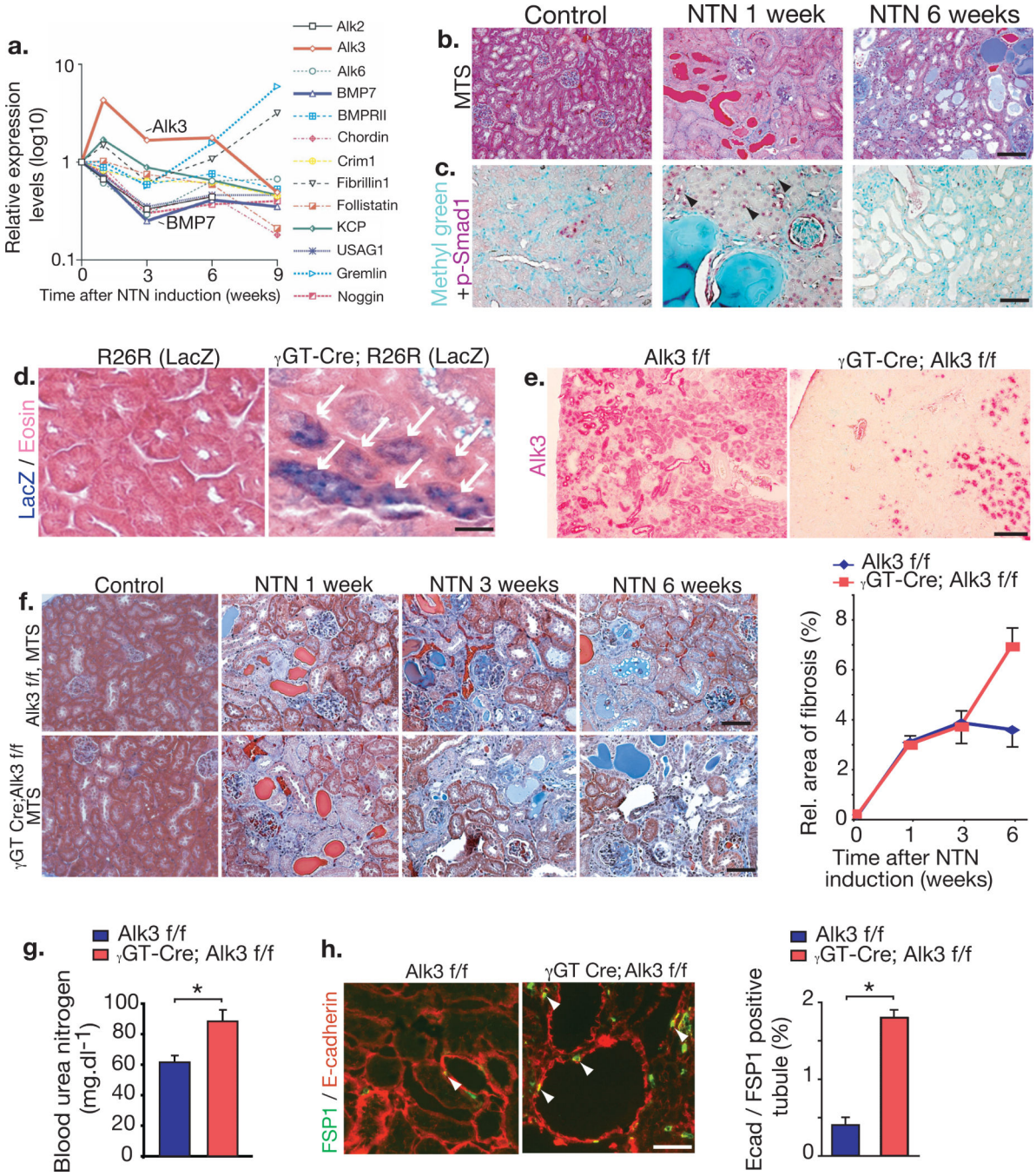

Figure 1. Alk3 and BMP7 expression inversely correlate in kidneys developing progressive injury and fibrosis

(**a**) Gene expression of indicated genes in kidneys of mice before (day 0) and after nephrotoxic serum nephritis (NTN) induction (1 week, 3 weeks, 6 weeks and 9 weeks after induction). (**b**) Representative MTS staining of control kidneys and kidneys from mice at one and six weeks following NTN. Scale bar: 50 μm. (**c**) Representative picture of kidneys from control mice and from mice at one and six weeks following NTN labeled with antibodies against phosphorylated Smad1 (p–Smad1). Scale bar: 50 μm. (**d**) Beta–

galactosidase substrate staining of kidneys of control mice (left) and γGT–Cre; R26R–Rosa–LSL–LacZ reporter mice (right) and eosin counter stain. Scale bar: 50 μm, arrows: positive LacZ staining. (**e**) Representative picture of kidneys from control Alk3 f/f (left) and γGT–Cre; Alk3 f/f mice (right) labeled with antibodies against Alk3. Scale bar: 100 μm. (**f**) Representative MTS staining (left) of NTN kidney from γGT–Cre; Alk3 f/f mice (n = 6) and littermate control mice (Alk3 f/f, n = 4) and morphometric quantification (right) of fibrosis in NTN kidney from control (Alk3 f/f) and γGT–Cre; Alk3 f/f mice. Scale bar: 50 μm. (**g**) Blood urea nitrogen measurement 60 days following NTN in γGT–Cre; Alk3 f/f mice (n = 5) and littermate control mice (n = 3). (**h**) Representative images for E–cadherin / FSP1 immunolabeling of kidneys from control (Alk3 f/f) and γGT–Cre; Alk3 f/f mice (left) and percent of E–cadherin / FSP1 double positive tubule (right). Scale bar: 25 μm. Data are expressed as mean ± s.e.m. * : $P < 0.01$.

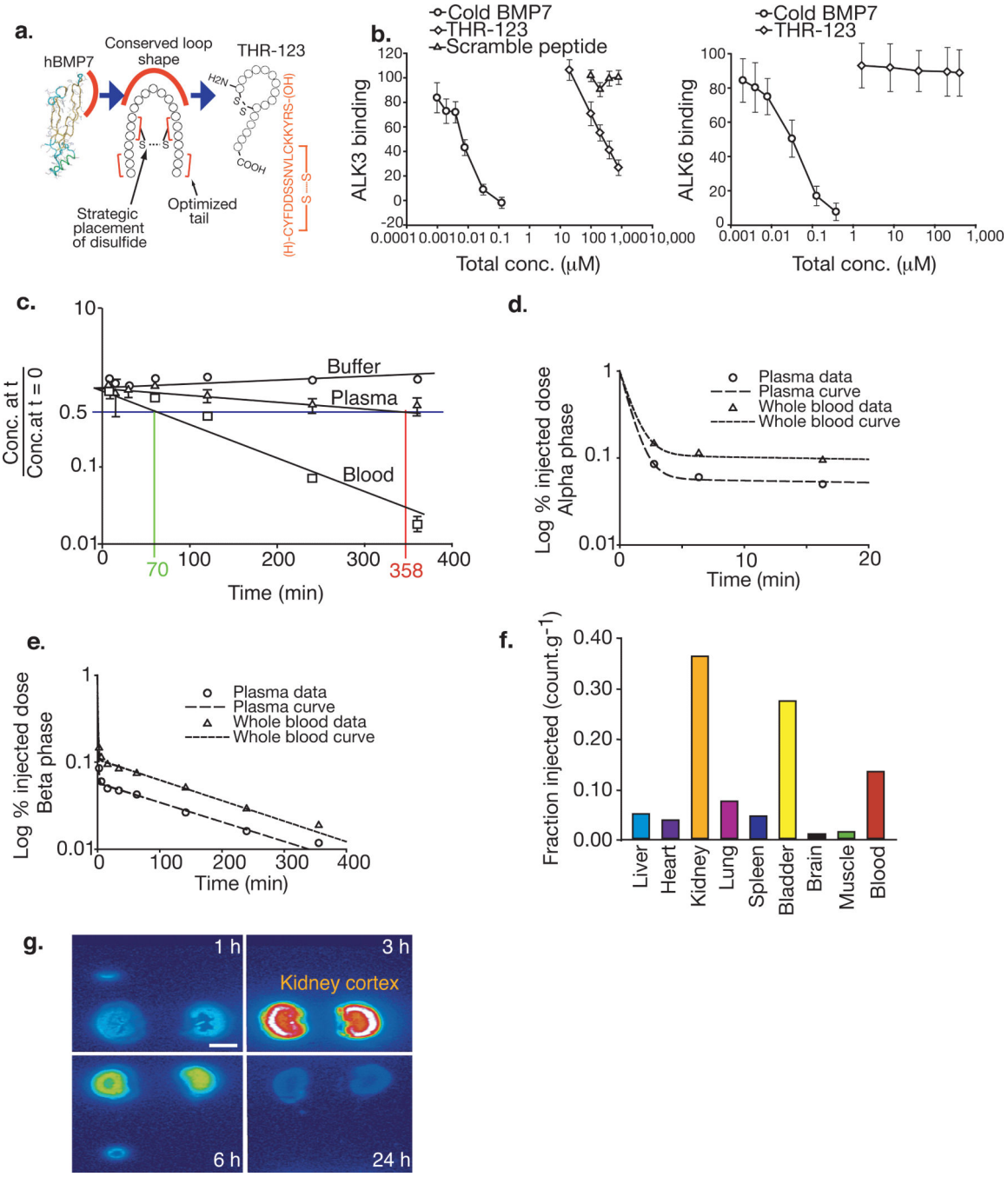

Figure 2. Synthesis and pharmacokinetics of THR–123

(**a**) Structure of BMP7 and THR–123. (**b**) Radio–ligand receptor competitive binding assays of THR–123 for Alk3 (left) and Alk6 (right) extra–cellular domain (ECD) (expressed as a fusion protein with Fc domain). (**c**) Stability of THR–123 in plasma and whole blood of rat following i.v. injection of ^{125}I–THR–123, data are expressed as the ratio of THR–123 concentration at the time of harvest (conc. at t) over THR–123 concentration at baseline (conc. at t = 0). (**d–e**) alpha phase (**d**) and beta phase (**e**) of THR–123 clearance in systemic circulation of rats following i.v. injection of ^{125}I–THR–123. (**f**). Tissue distribution of ^{125}I–

THR–123 six hours after i.v. administration. (**g**) Visualization of radioactivity of orally administrated ^{125}I–THR–123 in rat kidneys at 1, 3, 6 and 24 hours after administration. Scale bar: 15 mm. Data are expressed as mean ± s.e.m.

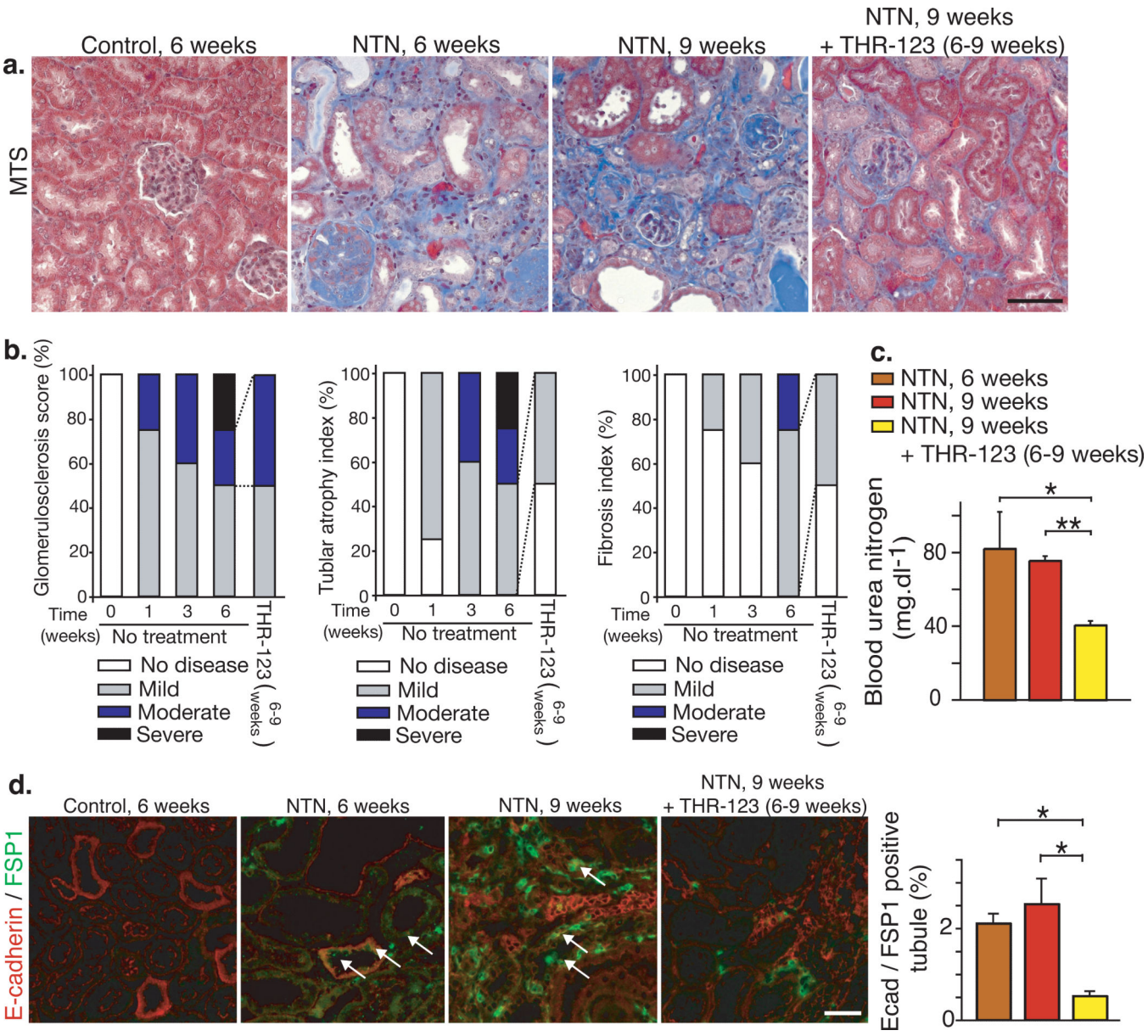

Figure 3. THR–123 reverses renal fibrosis in mice with nephrotoxic serum nephritis

(**a**) Representative MTS staining of kidney from untreated control mice (*n* = 5) (left panel); six weeks following NTN (*n* = 6, NTN, 6 weeks) (middle left panel); nine weeks post NTN (NTN, 9 weeks) (middle right panel); and nine weeks NTN with THR–123 administered starting at week 6 (NTN, 9 weeks + THR–123 (6–9 weeks)) (left panel), Scale bar: 40 μm. (**b**) Morphometric analysis from control mice (*n* = 5), mice after 1 (*n* = 6), 3 (*n* = 8), and six weeks following induction of NTN (*n* = 6), and mice at nine weeks following NTN with THR–123 administered starting six weeks following NTN (THR–123 (6–9 weeks) (*n* = 6)), assessing percent of glomerulosclerosis score (left), tubular atrophy index (middle), and fibrosis index (left). (**c**) Blood urea nitrogen measurement for mice six weeks following NTN (*n* = 3), nine weeks (*n* = 5), and nine weeks following NTN with THR–123 administered starting at week 6 following NTN (*n* = 5). (**d**) Representative images of E–

cadherin / FSP1 immunolabeling of kidney from control untreated mice (left panel), six weeks following NTN (middle left panel), nine weeks (middle right panel), and nine weeks following NTN with THR–123 administered starting at week 6 following NTN (right panel) and percent of E–cadherin / FSP1 double positive tubule assessed by counting the number of double–labeled tubules (right). Scale bar: 25 μm. Data are expressed as mean ± s.e.m. ** : $P < 0.01$, * : $P < 0.05$.

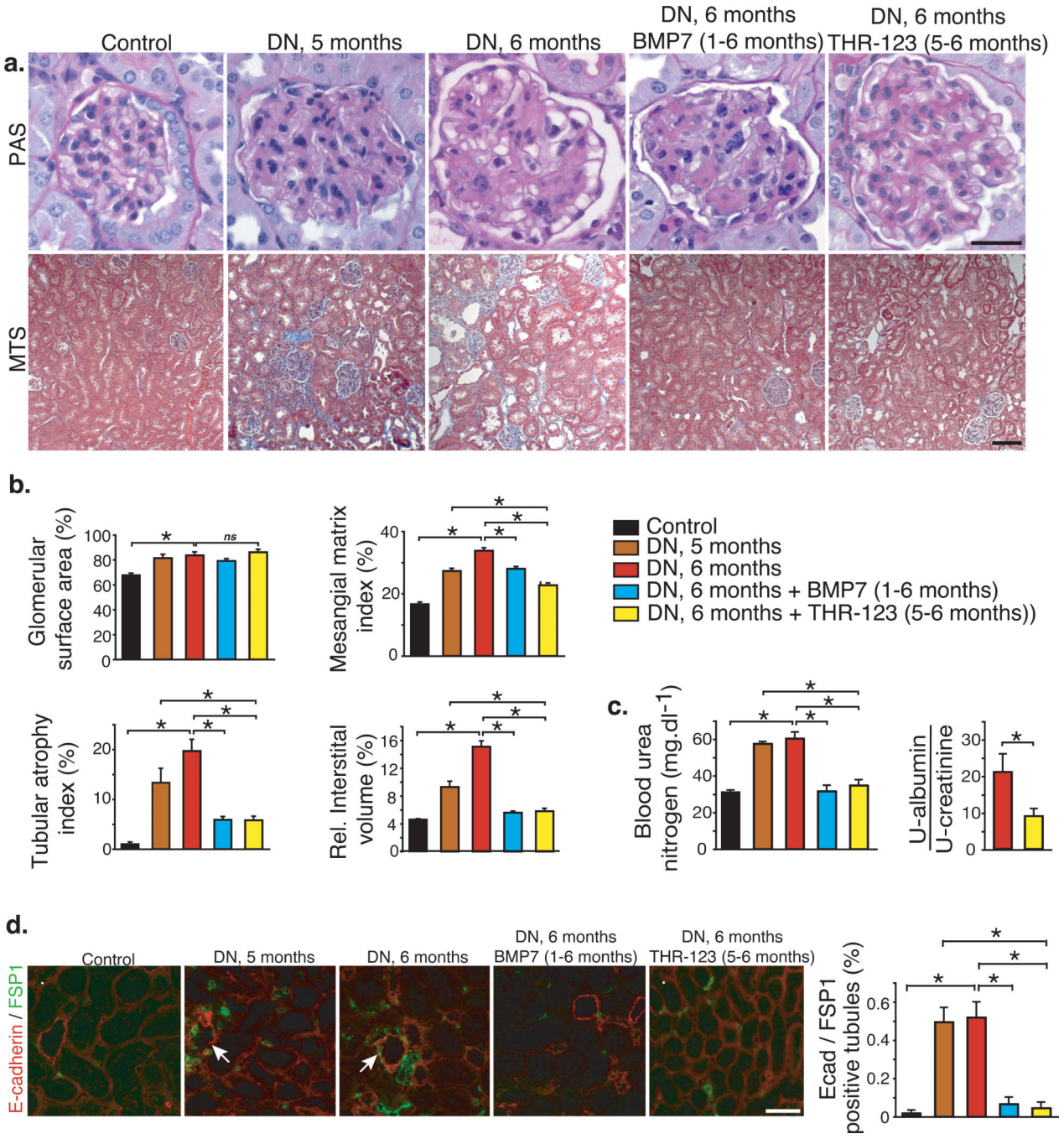

Figure 4. THR–123 reverses fibrosis associated with diabetic nephropathy

(**a**) Representative histological PAS (upper panels) and MTS (lower panels) staining of kidney sections of control mice (n = 5, left panel), five months following streptozotocin–induced diabetic nephropathy (DN) (n = 6, 2nd panel from the left), six months following DN (n = 10, middle panel), six months following DN and treated with BMP7 from one to six months following DN (n = 4, 4th panel) or THR–123 from five to six month following DN (n = 9, right panel). Scale bar upper panels: 10 μm, scale bar lower panels: 50 μm. (**b**) Morphometric analysis of glomerular surface area (top left), mesangial matrix (top right),

tubular atrophy (bottom left) and relative interstitial volume (bottom right). (**c**) Blood urea nitrogen measurement of control mice, five months following DN, six months following DN, six months following DN and treated with BMP7 from one to six months and six months following DN and treated with THR–123 from one to six months, and urine albumin over urine creatinine ratio of indicated experimental groups. (**d**) Representative images of E–cadherin / FSP1 immunolabeling of kidney of indicated experimental groups and percent of E–cadherin / FSP1 double positive tubule assessed by counting the number of double–labeled tubules. Scale bar 25 μm. Data are expressed as mean ± s.e.m. * : $P < 0.01$.

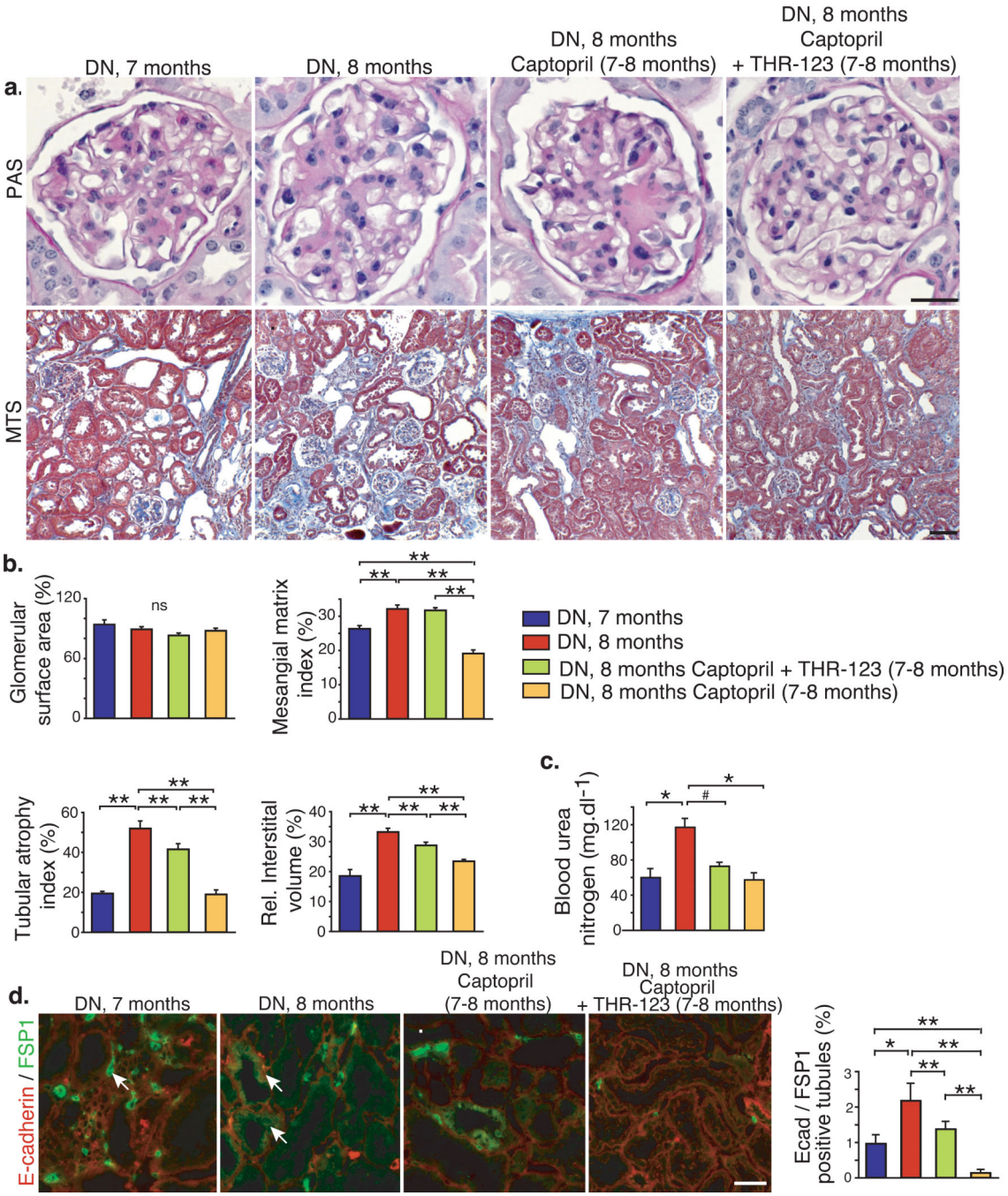

Figure 5. A combination of captopril and THR–123 inhibits progression of fibrosis associated with advanced diabetic nephropathy

(**a**) Representative histological PAS (upper panels) and MTS (lower panels) staining of kidney sections of mice seven months following streptozotocin–induced diabetic nephropathy (DN) (*n* = 2), eight months following DN induction (*n* = 3), eight months following DN induction and treated with captopril (CPR, *n* = 3), and eight months following DN induction and treated with combination of CPR and THR–123 (*n* = 4). Scale bar upper panels: 10 μm, scale bar lower panels: 50 μm. (**b**) Morphometric analysis of glomerular surface area (top left), mesangial matrix (top right), tubular atrophy (bottom left) and

relative interstitial volume (bottom right) of indicated experimental groups. (**c**) Blood urea nitrogen measurement in indicated experimental groups. (**d**) Representative images of E–cadherin / FSP1 immunolabeling of kidney from indicated experimental groups and percent of E–cadherin / FSP1 double positive tubules. Scale bar: 25 μm. Data are expressed as mean ± s.e.m. ** : $P < 0.01$, * : $P < 0.05$, # : $P = 0.08$, ns: not significant.

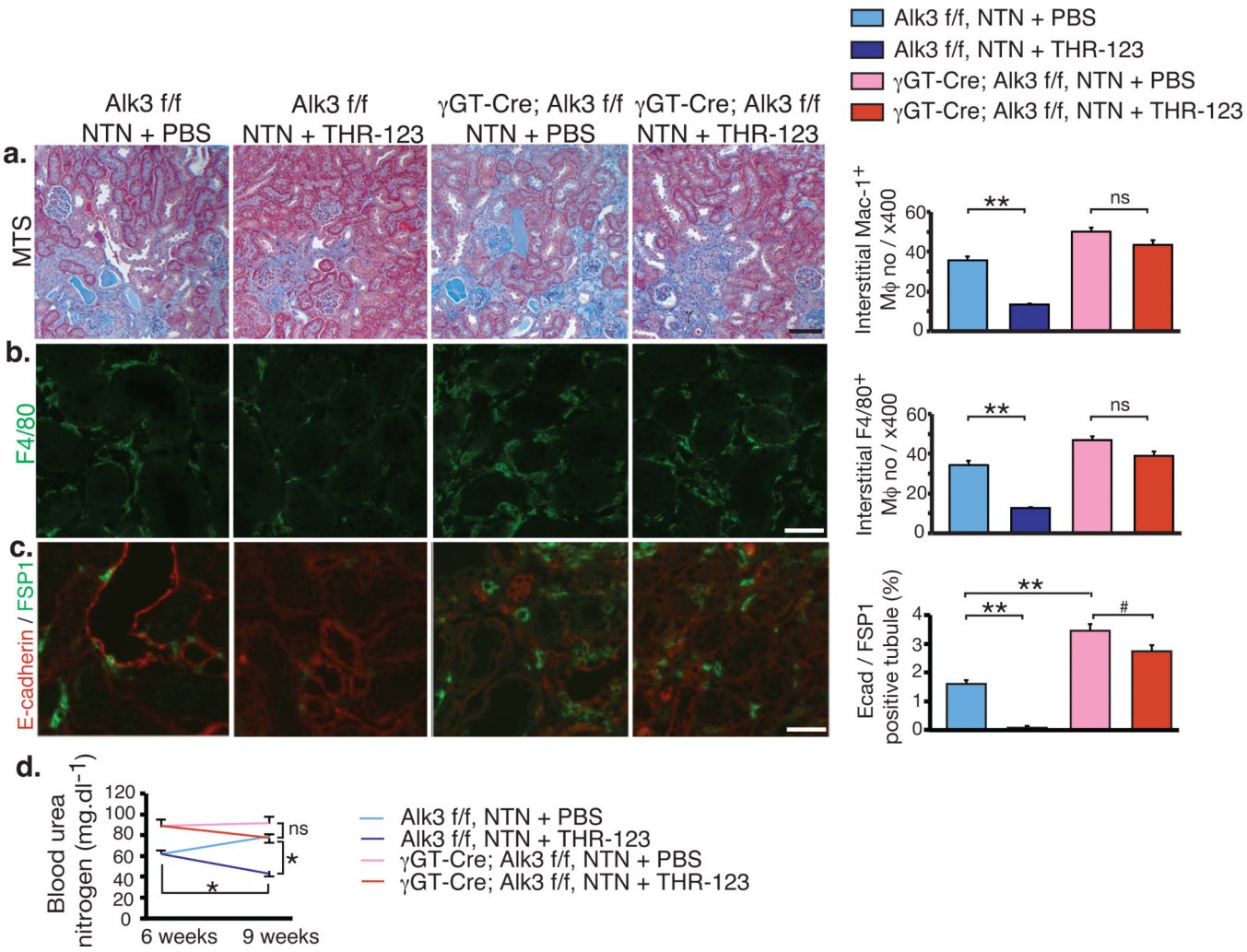

Figure 6. Alk3 is a functional receptor for the activity of THR–123

(**a**) Representative MTS staining picture of Alk3 f/f and γGTCre; Alk3 f/f mice six weeks after NTN and treated with PBS or THR–123 (*n* = 4 in each group). And morphometric analyses of interstitial fibrosis in kidneys of mice the indicated experimental groups. Scale bar: 50 μm. (**b**) Representative images of F4/80 immunofluorescence in the indicated experimental groups and quantitation of the number of F4/80^{+} macrophages (Mφ) per field of view. Scale bar: 25 μm. (**c**) Representative images of E–cadherin / FSP1 immunolabeling of kidney from indicated experimental groups and percent of E– cadherin / FSP1 double positive tubules. Scale bar: 25 μm. (**d**) Blood urea nitrogen measurement in six and nine weeks of NTN in indicated experimental groups (all *n* = 4). Data are expressed as mean ± s.e.m. ** : $P < 0.01$, * : $P < 0.05$. ns: not significant.